Biomacromolecules

Article

Cite This: Biomacromolecules XXXX, XXX, XXX−XXX

pubs.acs.org/Biomac

Superstrong and Tough Hydrogel through Physical Cross-Linking and Molecular Alignment

Wei Chen,[†,‡,⊥] Nan Li,[†,‡,⊥] Yi Ma,[†] Marilyn L. Minus,[†] Kenneth Benson,[†] Xiuling Lu,[§] Xingzhi Wang,[∥] Xi Ling,[∥] and Hongli Zhu*[,†]

[†]Department of Mechanical and Industrial Engineering, Northeastern University, Boston, Massachusetts 02215, United States

[‡]College of Engineering, Qufu Normal University, Rizhao 276826, China

[§]Department of Pharmaceutical Sciences, University of Connecticut, Storrs, Connecticut 06269, United States

[∥]Department of Chemistry, Boston University, Boston, Massachusetts 02215, United States

Supporting Information

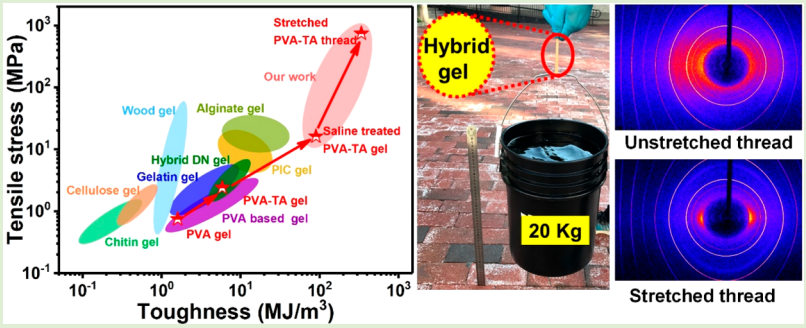

ABSTRACT: Hydrogels are attracting increasing attention due to their potential use in various fields. However, most of the existing hydrogels have limitations in either dissipating mechanical energy or maintaining high stretchability under deformation, thus do not possess high mechanical properties. Herein, poly(vinyl alcohol) (PVA)−tannic acid (TA) hydrogels with both high mechanical strength and stretchability were obtained via a step-by-step physical cross-linking and molecular alignment method. Saline-triggered physical interactions serve as "sacrifice domains" to dissipate energy and endow PVA-based hydrogel with high mechanical strength (≈16 MPa) and stretchability (≈1000%). Due to the reversible arranging and disassociating property of physical interactions, PVA−TA hydrogels show excellent shape memory performance. We further demonstrated an effective approach to fabricate strong and aligned PVA−TA thread. The resultant well-aligned PVA−TA dry thread reveals an ultrahigh mechanical tensile strength of up to 750 MPa, nearly 45 times higher than PVA−TA thread with no alignment. Wide-angle X-ray two-dimensional diffraction images further confirmed the alignment of PVA fibers in stretching direction. In addition, we applied the PVA−TA hydrogel as suture and evaluated the cytotoxicity and biocompatibility of the PVA−TA suture.

INTRODUCTION

As one of the most important soft materials, hydrogels have been widely applied in modern technologies, including tissue engineering,[1,2] drug delivery,[3,4] sensors,[5] actuators,[6] etc. Compared to hard and brittle polymeric materials, hydrogels are soft and deformable, and thus attracted broad attention. Because amorphous polymer chains endow hydrogels with high flexibility or "softness", they lead to inferior mechanical performances, which frequently hampers their practical applications. Over recent years, significant efforts have been made to increase the mechanical strength of hydrogels, and methodologies include double-network,[7] tetra-arm polymer hydrogels,[8] hybrid chemical and physical hydrogels,[9,10] macromolecular microsphere composite hydrogels,[11] and slide-ring hydrogels.[12] However, most of these developed tough hydrogels were inferior to biological tissues such as ligaments, tendons, and cartilages in many aspects.[13,14]

Inspired by nature and biology, various synthetic hydrogels with aligned structures can now be made as tough as or even much tougher than natural tissues. For example, Gong's group[15] reported the fabrication of anisotropic hydrogels with both high strength (up to 54 MPa) and toughness (up to 40 MJ/m^3) by drying in confined condition method. Wu et al.[16] prepared a type of bioinspired fibers by drawing from a hydrogel at ambient temperatures and pressures. The fibers were much tougher than natural tissues with tensile strengths up to 200 MPa and toughness up to 30 MJ/m^3. Very recently, Wang's group[17] has reported a type of strong and tough poly(vinyl alcohol)/poly(acrylic acid) (PVA/PAA) hydrogel by immersing the as-prepared PVA hydrogels in aqueous PAA solution and then cold-drawing the hydrogels with different

Received: September 4, 2019
Revised: October 19, 2019
Published: October 23, 2019

DOI: 10.1021/acs.biomac.9b01223
Biomacromolecules XXXX, XXX, XXX−XXX

strains. The tensile strength and toughness of cold-drawn fibers are up to 140 MPa and 117 MJ/m^3, respectively. Nevertheless, such approaches to generate aligned structures are either time-consuming or have poor biocompatibility, low biodegradability, and may generate potential toxicity during use. Therefore, it still remains a challenge to explore hydrogels with good biocompatibility as well as high mechanical properties comparable or even superior to those of biological tissues. Recently, a straightforward soaking treatment method has ben widely used and its effectiveness has been demonstrated on various hydrogel systems, including poly(acrylic acid)-Fe^{3+} and poly(vinyl alcohol) hydrogels.[18,19] Compared to other strategies that involve complicated chemistry and/or manufacturing, the soaking method is much simpler and reproducible.

Poly(vinyl alcohol) (PVA) is a water-soluble, nontoxic, biocompatible, and biodegradable synthetic green material. Because of its many advantages, PVA hydrogels have been widely used in the field of biomedicine.[20] Tannic acid (TA), a naturally occurring water-soluble polyphenol, could be found in red wine, tea, grapes, chocolate, and in the bark of many plants.[21] The literature shows that TA can be an effective gelation binder to cross-link PVA into hydrogels due to the strong hydrogen bonds (H-bonds) formed between these two polymers.[22,23] Nonetheless, tensile strengths of these developed PVA−TA hydrogels were less than 10 MPa, inferior to those of biological hydrogels and plastics, due to the lack of effective energy dissipations and ordered structures.

In this work, we use a classic freezing/thawing method, freezing below 0 °C and then thawing at ambient temperature, to obtain PVA−TA hydrogels with crystalline domains. Through simply soaking in NaCl solution, these gels exhibit good mechanical performances because of the formation of chain entanglements due to the salting-out effect.[33,34] When immersed in water, these newly formed physical interactions could disassociate automatically (Scheme 1a). In addition, a surgical wound suture was prepared by injecting PVA−TA solution into NaCl solution and stretching (Scheme 1b). By applying a stretching force, the stretched thread shows a record-high toughness and fracture strength among those reported tough materials (Scheme 1c). We further evaluated the cytotoxicity and biocompatibility of the PVA−TA suture. We anticipate that this work could inspire other researchers producing multifunctional PVA−TA products for various applications in bioengineering.

EXPERIMENTAL SECTION

Materials. PVA (M_w: 146 000−186 000 g/mol, >99% hydrolysis) was purchased from Sigma-Aldrich, Inc. Tannic acid, 95% (TA) and NaCl were purchased from Fisher Inc.

Preparation of PVA−TA-Based Hydrogels. A desired amount of TA powder (0−60 wt % to PVA) was dissolved in deionized water (17.1 mL). After complete dissolution, 6 g of PVA powder was slowly added and mixed with TA solution. The mixed solution was then heated to ∼95 °C to dissolve PVA under vigorous stirring. In the whole heating process, the system was sealed to prevent water evaporation. Then, the mixture was cast into a lab-made glass mold to form gels via a classic freezing/thawing method (i.e., cooling to −15 °C for 2 h and then thawed at room temperature). Finally, the as-prepared PVA−TA hydrogels were soaked in NaCl solution for 12 h to prepare condensed PVA−TA hydrogels. The composition of saline-treated gels was referred to as PVA−TA x−y NaCl, where x is the concentration of TA to PVA (% w/w) and y is the concentration of NaCl (% w/w). "S" stands for the saturated concentration of NaCl solution. For example, PVA−TA 30−20% NaCl meant TA was 30 wt % PVA and the concentration of NaCl was 20%; PVA−TA-30%-S-NaCl (where S stands for immersed in saturated NaCl) meant TA was 30 wt % PVA and the concentration of NaCl solution was saturated.

Scheme 1. (a) Conceptual Illustration of the Synthesis Procedure of Saline-Treated PVA−TA Hydrogels. Physical Interactions Triggered by Saline is Reversible. (b) Wet-Drawing PVA−TA Thread in Aqueous Sodium Chloride (NaCl) Solution. The Resultant Thread Could Generate Alignments by Immediately Stretching. (c) Our Work is Compared to Other Reported Tough Materials, Including Cellulose Hydrogel,[24] Chitin Hydrogel,[25] Gelatin Hydrogel,[26] Hybrid Double Network (DN) Hydrogels,[9,27] Alginate Hydrogel,[15] PVA-Based Hydrogels,[28,29] Wood Hydrogel,[30] and Polyelectrolyte (PIC) Hydrogels.[31,32]

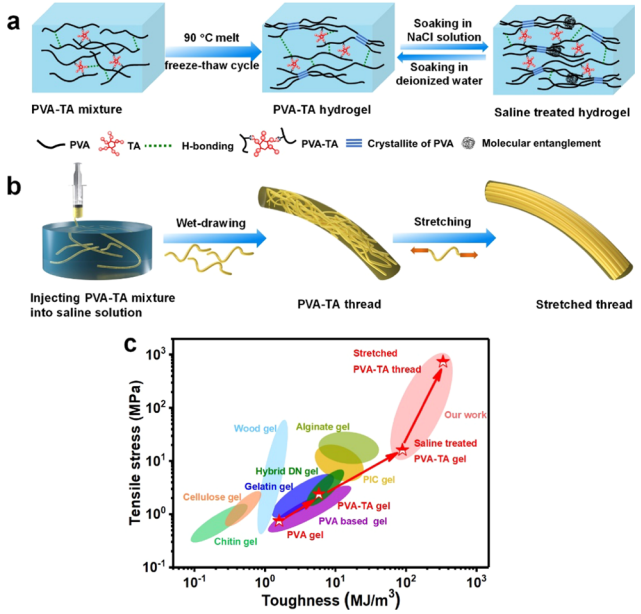

Preparation of PVA−TA Threads. A manual syringe was used to inject PVA−TA mixtures into saturated NaCl solution. Thereafter, by immediately applying a stretching force, stretched PVA−TA threads were obtained without freezing/thawing treatment.

Water Content and Swelling Ratio Test. Water contents (WC) were determined from the equation

$$\mathrm{WC} = \frac{(W_w - W_d)}{W_d} \times 100\% \quad (1)$$

where W_w and W_d are the weight of the as-prepared and dry samples, respectively.

The swelling properties of the hydrogels were measured as follows: about 1.0 g of dried sample was immersed in distilled water at room temperature. After predetermined times, the hydrogel was taken out using an absorbent paper wiping water on its surface and weighed. The swelling ratios (SRs) were calculated according to the following equation

$$\mathrm{SR} = \frac{W_s - W_d}{W_d} \quad (2)$$

where W_d and W_s are the weight of dried and swollen samples, respectively.

Mechanical Measurements. The mechanical properties of hydrogels (3 mm width × 12 mm length × 2 mm thickness) were tested using an Instron Model 5567 Machine with a crosshead speed of 100 mm/min at room temperature. The tensile hysteresis was measured on the hydrogels under elongation below 800%. The elastic

DOI: 10.1021/acs.biomac.9b01223
Biomacromolecules XXXX, XXX, XXX−XXX

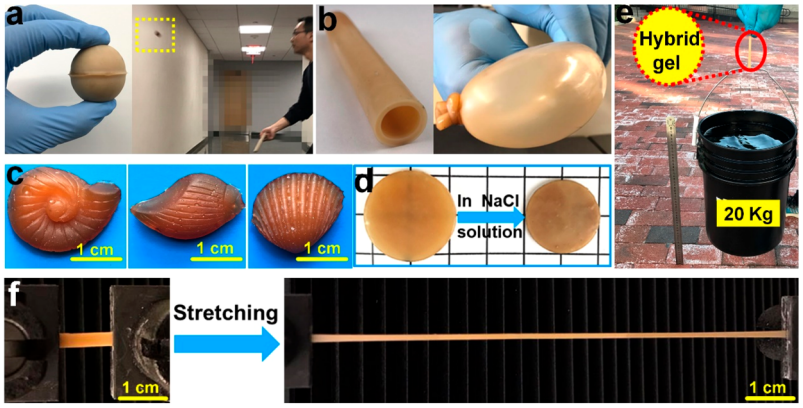

Figure 1. Photographs of (a) a PVA−TA-30% hydrogel ball (d = 4 cm, left) could be hit like a "ping-pong" ball (right), (b) a PVA−TA-30% hydrogel tube (left) blown into a balloon (right), and (c) the PVA−TA-30% hydrogels with different seawater animal shapes. (d) Visual appearances of PVA−TA-30% and PVA−TA-30%-S-NaCl hydrogels. (e) PVA−TA-30%-S-NaCl hydrogels sheet with a width of 10 mm and thickness of 1.9 mm could bear a bucket of water of about 20 kg in weight. (f) Outstanding stretching performance of PVA−TA-30%-S-NaCl hydrogel sheet (stretching over 1000%).

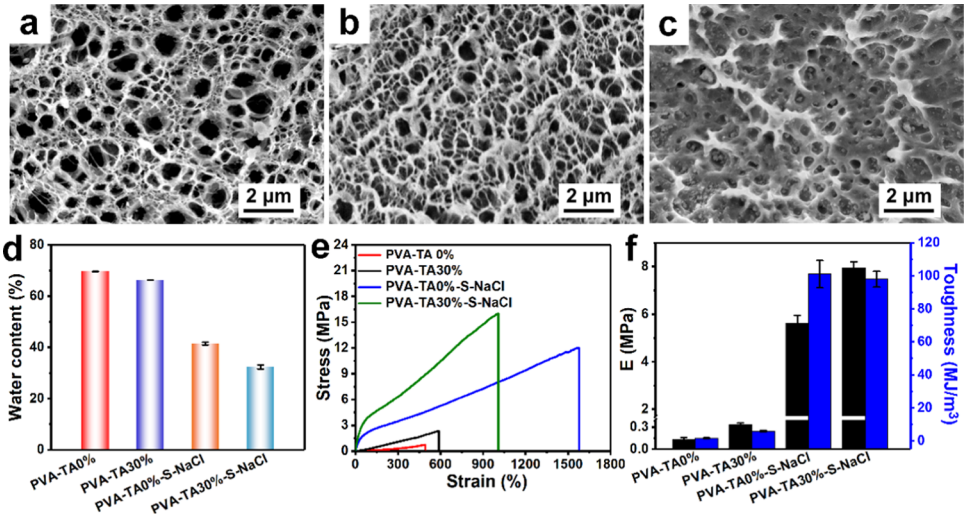

Figure 2. SEM images o((a) PVA−TA-0%, (b) PVA−TA-30%, and (c) PVA−TA-30%-S-NaCl hydrogels. (d) Water contents, e) tensile stress−strain curves, and (f) elastic moduli and toughnesses of PVA−TA-0%, PVA−TA-30%, PVA−TA-0%-S-NaCl, and PVA−TA-30%-S-NaCl hydrogels.

modulus (E) was calculated from the linear regions (ε_t = 5−10%) of the tensile stress−strain curves. The toughness of hydrogels was calculated as the area under tensile stress−strain curves. The dissipated energy (hysteresis, U_{hys}) was calculated as the area between the loading−unloading curves. Before each tensile test experiment, silicon oil was coated on the hydrogel to prevent water evaporation.

Shape-Memory Observation. For the shape-fixing process, PVA−TA hydrogel with a straight strip (permanent shape) was curled into a tight helix shape (temporary shape) and then immersed in NaCl solution for a certain time. For the shape recovery process, the deformed helix strip was transferred to deionized water. The shape fixity ratios (R_f) and shape recovery ratios (R_r) of PVA−TA hydrogels were calculated using the following equations

$$R_f = \frac{\theta_t}{\theta_i} \times 100\% \quad (3)$$

$$R_r = \frac{\theta_i - \theta_f}{\theta_t} \times 100\% \quad (4)$$

where θ_i is the actually curled angle, θ_t is the temporarily fixed angle, and θ_f is the final angle.

Characterization. For the measurement of attenuated total infrared spectroscopy (ATR-FTIR), hydrogels were dried to eliminate water. The ATR-FTIR spectra were recorded in the wavenumber range of 4000−500 cm^{-1} using a Bruker FT-IR Vertex 70 spectrometer. Raman spectroscopy and spatial Raman mapping were performed using a Raman imaging microscope (Horiba-JY T64000). The collected spectra were preprocessed using cosmic ray removal, noise filtering, and normalization techniques to collect Raman maps (maximum scan range ≈ 20 × 20 μm^2). The surface morphologies of hydrogels were investigated using an emission scanning electron microscope (Hitachi S4800). Wide-angle X-ray diffraction (WAXRD) data and 2D diffraction patterns were recorded on a Rigaku RAPID II equipped with a curved detector manufactured by Rigaku Americas Corp. (operating tube voltage: 40 kV; tube current: 30 mA, Cu Kα, λ = 0.1541 nm).

Cell Cultivation. The PVA−TA-30% hydrogels (control group) and dialyzed PVA/TA sutures were exposed to ultraviolet light for 30 min. The samples were then placed on a well of a 12-well plate and washed with sterilized physiological saline for 30 min. The mouse Leydig tumor cell line (I-10) was maintained in F12 medium with 15% horse serum and 2.5% fetal bovine serum at 37 °C and 5% CO_2. Cell culture reagents were purchased from Invitrogen Life Technologies (Carlsbad, CA). Thereafter, I-10 cells (1.0×10^4 cells) were cultured on the surface of the PVA/TA suture at a density of 1×10^4 cells per well. The viability of the cells was determined using a LIVE/DEAD Viability/Cytotoxicity Kit (MesGen

DOI: 10.1021/acs.biomac.9b01223
Biomacromolecules XXXX, XXX, XXX−XXX

Biotech, MCT8010-100T) and visualized with a fluorescence microscope (Axio Observer Z1, ZEISS, Germany).

Implantation of PVA/TA Suture for Immune Response in a Mouse Model. All animal care and experimental procedures followed the animal use protocols and were approved by the Institutional Animal Care and Use Committee of Qufu Normal University (dwll2019080101). Mice (ICR, male, 4 weeks) were obtained from Jinan Pengyue Laboratory Animal Co., Ltd. (Shangdong, China). These mice were anesthetized with pentobarbital sodium. Subsequently, the PVA/TA sutures were implanted in connective tissues in dorsum. After 3 days, the mice were euthanized and the connective tissues were dissected and embedded in optimal cutting temperature (OCT) compound. These tissues were stained with routine hematoxylin and eosin (H&E) stain.

RESULTS AND DISCUSSION

Appearances and Mechanical Performances of PVA−TA Hydrogels. As shown in Figure 1a, a PVA−TA-30% hydrogel ball could withstand repeated hit and bounce without a rupture (Movie S1), and a PVA−TA-30% hydrogel tube could be repeatedly browned into a balloon via an air pump (Figure 1b and Movie S2), suggesting that the PVA−TA-30% hydrogels possessed good mechanical properties. Besides, PVA−TA hydrogels could readily form various sea animal shapes (Figure 1c), indicating its free-shapable property. After immersed in saturated NaCl solution, the PVA−TA-30%-S-NaCl (where S stands for immersed in saturated NaCl) hydrogel shrinked and a similar phenomenon could be observed for PVA−TA-0%-S-NaCl hydrogel (Figures 1d and S1). Remarkably, PVA−TA-30%-S-NaCl hydrogels could bear a full bucket of water with 20 kg weight and stretched to over 1000% of its original length (Figure 1e,f), demonstrating its ultrahigh strength and stretchability.

The microstructures of various PVA hydrogels were observed by scanning electron microscopy (SEM). For PVA−TA-0% hydrogel, the distribution of the pore was uniform and the size of the pore was more than 600 nm (Figure 2a). After adding TA, the pore size slightly decreased (Figure 2b). Compared to PVA−TA-0% and PVA−TA-30% hydrogels, PVA−TA-30%-S-NaCl hydrogel had the smallest pore size (Figure 2c), suggesting the formation of a denser structure. Water contents had a crucial impact on the structures and mechanical properties of hydrogels: lower water content usually means denser and smaller pore structure. It can be seen from Figure 2d that the water contents decreased significantly from 69.5 and 66.2% for PVA−TA-0% and PVA−TA-30% hydrogels to 41.5 and 32.4% for PVA−TA-0%-S-NaCl and PVA−TA-30%-S-NaCl hydrogels, respectively. The degrees of equilibrium swelling of PVA-based hydrogels were also measured to further reveal the structural features of hydrogels. As shown in Figure S2, compared to PVA−TA-0% and PVA−TA-30% hydrogels, PVA−TA-0%-S-NaCl and PVA−TA-30%-S-NaCl hydrogels exhibited lower equilibrium swelling ratios (SR (g/g), 0.69 and 0.64, respectively) and smaller volume expansion, which were ascribed to the denser network structure of the saline-treated hydrogels.

PVA−TA-30%-S-NaCl hydrogel possesses good mechanical properties. As shown in Figures 2e and S3, the interactions induced by the salting-out effect of NaCl solution endow the PVA−TA-30%-S-NaCl hydrogel with superior mechanical properties. The compressive stress at a compressive strain of 90% was 5.9 and 7.9 MPa for PVA−TA-0% and PVA−TA-30% hydrogels, respectively. After treatment with saturated NaCl solution, a significant enhancement in the compressive strength occurred, with high compressive stresses at the compressive strain of 85% of 18.2 and 24.7 MPa for PVA−TA-0%-S-NaCl and PVA−TA-30%-S-NaCl hydrogels, respectively. The elongation and tensile strength of PVA−TA-30%-S-NaCl were about 1000% and 16 MPa, which were 2 and 22 times higher than that of PVA−TA-30% hydrogel, respectively. Moreover, different from the weak elastic moduli and small toughnesses of PVA−TA-0% (elastic modulus ≈ 0.1 MPa, toughness ≈ 1.6 MJ/m^3) and PVA−TA-30% hydrgoels (elastic modulus ≈ 0.3 MPa, toughness ≈ 5.9 MJ/m^3), the PVA−TA-30%-S-NaCl hydrogels exhibit stronger elastic moduli and toughnesses (Figure 2f). Their good mechanical properties can be attributed to the following aspects: first, the increased density and smaller pores of PVA−TA-30%-S-NaCl hydrogel could avoid stress concentration and crack expanding. Second, during deformation, the saline-induced physical interactions were de-cross-linking and serving as "sacrificial domains" to dissipated mechanical energy and rendered hydrogel high tensile strength.[35]

Key Parameters Affect the Mechanical Properties and Energy Dissipation Capacities of PVA−TA Hydrogels. To gain more insight into the reinforcement mechanism of PVA−TA hydrogels, we prepared hydrogels with different TA contents by using various cycles of freezing/thawing method and sequentially immersing in NaCl solution for different times and concentrations. The effect of various TA contents, freezing/thawing cycles, immersing times, and NaCl concentrations on the mechanical properties of PVA−TA hydrogels are presented in Figure S4. As expected, higher TA contents result in higher tensile strength and elongation (Figure S4a). After being immersed in saturated NaCl solution (12 h), all hydrogel samples displayed significant improvements of tensile strength, elongation (Figure S4b), as well as high elastic moduli (Figure S4c) and toughnesses (Figure S4d). Nevertheless, there were no obvious changes observed by increasing the number of freezing−thawing cycles (Figure S5a,b), suggesting that with respect to a relatively strong physical interaction, an enhanced crystallization network could be ignored. In addition, the mechanical strength of hydrogels could be easily tuned by changing immersing time and the concentration of NaCl solutions, as demonstrated in Figure S5c−f. The dissipation energies of PVA−TA hydrogels were measured by loading−unloading tests to obtain further insight into the energy dissipation mechanisms during deformation. Generally, the hysteresis loop area represents energy dissipation. A comparison between PVA−TA-0%, PVA−TA-30%, PVA−TA-0%-S-NaCl, and PVA−TA-30%-S-NaCl hydrogels at the same strain (400%) are presented in Figure 3a,b. As clearly shown, the saline-treated PVA hydrogels have more pronounced hysteresis loops than untreated PVA hydrogels. More specifically, by fixing the strain at 400%, the PVA−TA-0%-S-NaCl and PVA−TA-30%-S-NaCl hydrogels consumed energy as much as 10.1 and 14.4 MJ/m^3, respectively, which were 84.8 and 86.1% of the total works (Figure 3b). In conclusion, compared to those untreated hydrogels, the saline-treated hydrogels dissipated more energy. When immersed in NaCl solution, the hydrogel is dehydrated, and the shrinkage of the hydrogel led to a closer contact of TA and PVA chains, as well as individual PVA and TA chains. Very possibly, during this process, a densified structure is formed, where ions are surrounded by entangled PVA and TA chains in the molecular spaces.[36,37] Because a large amount of energy is required to break this structure, the mechanical properties of the PVA−

DOI: 10.1021/acs.biomac.9b01223
Biomacromolecules XXXX, XXX, XXX−XXX

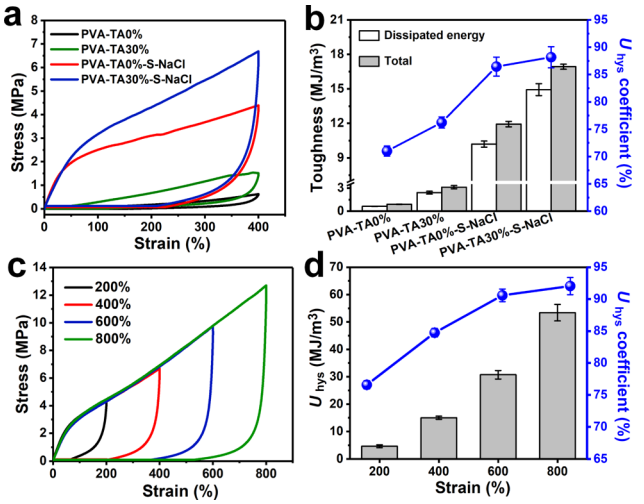

Figure 3. (a) Loading−unloading curves and (b) the corresponding dissipated energy and dissipation coefficient of PVA−TA-30%-S-NaCl hydrogel during loading−unloading tests. (c) Loading−unloading curves and (d) the corresponding dissipated energy and dissipation coefficient of PVA−TA-30%-S-NaCl hydrogels under different strains (200, 400, 600, and 800%).

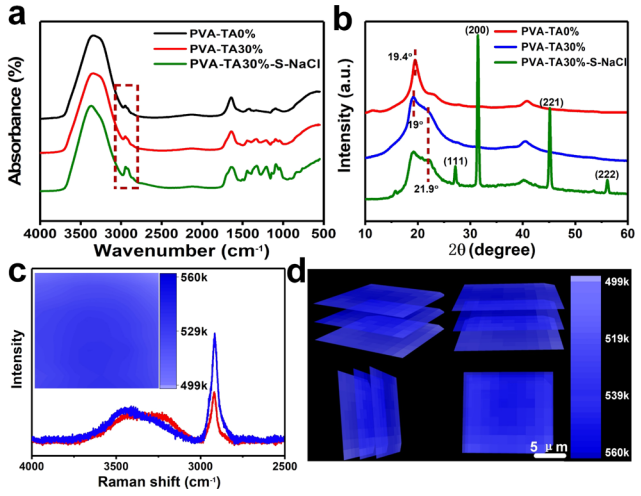

Figure 4. (a) ATR-FTIR spectra and b) X-ray diffractions of PVA−TA-0%, PVA−TA-30%, and PVA−TA-30%-S-NaCl hydrogels. (c) Raman spectra of PVA−TA-0% (red curve) and PVA−TA-0%-S-NaCl hydrogels (blue curve). The inset is the reconstructed Raman image obtained from the Raman intensity of C−H stretching mode intensities at 2900 cm^{-1}. Deep blue corresponds to the C−H-rich regions, and light blue indicates C−H-poor domains. (d) Three-dimensional (3D) Raman images of PVA−TA-0%-S-NaCl hydrogel.

TA-30%-S-NaCl hydrogels are significantly improved. This was one possible toughening mechanism of PVA−TA-30%-NaCl hydrogels.

Next, we further investigate the energy dissipation capacities of PVA−TA-30%-S-NaCl hydrogels. As presented in Figure 3c, with the increase of strain, the hysteresis energy of PVA−TA-30%-S-NaCl hydrogels became more remarkable. The quantified results are shown in Figure 3d. With an increase in strain from 200 to 800%, one can note that the PVA−TA-30%-S-NaCl hydrogels could dissipate more significant energy and achieve a higher energy dissipation ratio. For example, the hysteresis energy increased from 4.5 MJ/m^3 at 200% to 52.2 MJ/m^3 at 800% and the dissipation coefficient increased from 76.6 at 200% strain to 92.7% of the total work at 800% strain.

Characterizations of PVA−TA Hydrogels. To understand the nature of the PVA-based hydrogels, we analyzed the total reflection (ATR)−Fourier transform infrared (FTIR) spectra of PVA−TA-0%, PVA−TA-30%, and PVA−TA-30%-S-NaCl hydrogels. As shown in Figure 4a, PVA−TA-0% hydrogel has characteristic peaks at around 3263 cm^{-1} for O−H stretching, at about 2900 cm^{-1} for C−H stretching, and at around 1095 cm^{-1} for C−O stretching.[38] With the addition of TA, the O−H stretching absorption peak at 3263 cm^{-1} shifted to lower wavenumber. The red shift of the O−H stretching peak indicates that H-bonds exist between TA and PVA.

However, compared to PVA−TA-0% and PVA−TA-30% hydrogels, the −OH peak of PVA−TA-30%-S-NaCl hydrogel shifted to higher wavenumber. It is widely believed that the addition of NaCl decreases the extent of H-bonds and disrupts the hydrogen-bonded structure.[36,39] Nonetheless, the situation is more intricate for PVA−TA-30%-S-NaCl hydrogel system since H-bonds not only exit between PVA chains and water molecules but also between PVA and TA chains, as well as within individual PVA chains and TA chains. In the PVA−TA-30%-S-NaCl hydrogel system, NaCl probably disrupted both inter- and intramolecular H-bonds and densified the hydrogel, leading to the entanglements of PVA and TA chains.[36] Besides, the peak at about 2900 cm^{-1}, known as the C−H stretching bond, was enhanced after immersed in NaCl solution, which was due to the formation of new physical interactions. Furthermore, there was no appearance of new vibration, indicating that no new covalent bond formed in PVA−TA-30% and PVA−TA-30%-S-NaCl hydrogels.

Wide-angle X-ray diffraction (WXRD) patterns of the PVA−TA-0%, PVA−TA-30%, and PVA−TA-30%-S-NaCl hydrogels were further examined. As can be noted from Figure 4b, the WXRD pattern of PVA−TA-0% hydrogel shows a sharp diffraction peak at 2θ = 19.4°, which is ascribed to a typical semicrystalline PVA.[40] For PVA−TA-30% hydrogel, the diffraction peak at 19.4° shifted to 19° due to new H-bonds formed between PVA and TA. Moreover, compared to PVA−TA-0% hydrogel, PVA−TA-30% and PVA−TA-30%-S-NaCl hydrogels displayed new diffraction peaks at 21.9°. Notably, the diffraction intensity of the 21.9° peak of PVA−TA-30%-S-NaCl hydrogel was stronger than that of PVA−TA-30% hydrogel. This observation indicated that a more compact crystalline structure formed in the PVA−TA-30%-S-NaCl hydrogel. Besides, diffraction peaks for the (111), (200), (221), and (222) planes of PVA−TA-30%-S-NaCl hydrogel were attributed to NaCl crystals.

Figure 4c showed that the O−H stretching vibrational mode shifted from 3445 cm^{-1} in PVA−TA-0%-S-NaCl to 3419 cm^{-1} in PVA−TA-0% hydrogel. Additionally, the intensity of the C−H stretching mode (2900 cm^{-1}) was enhanced. These shifted and enhanced absorption peaks in Raman spectroscopy further confirmed that physical interactions chain entanglements exist in PVA−TA-0%-S-NaCl hydrogel. Besides, it can be observed from the Raman mapping image that the physical interactions were almost uniformly distributed. The reconstructed 3D Raman images further confirmed the homogeneous distribution of the newly formed physical interactions in PVA-TA-30%-S-NaCl hydrogels (Figure 4d).

Shape-Memory Properties. The robust and biocompatibility properties of saline-treated PVA-based hydrogels enable us to explore its various properties and applications. For

DOI: 10.1021/acs.biomac.9b01223
Biomacromolecules XXXX, XXX, XXX−XXX

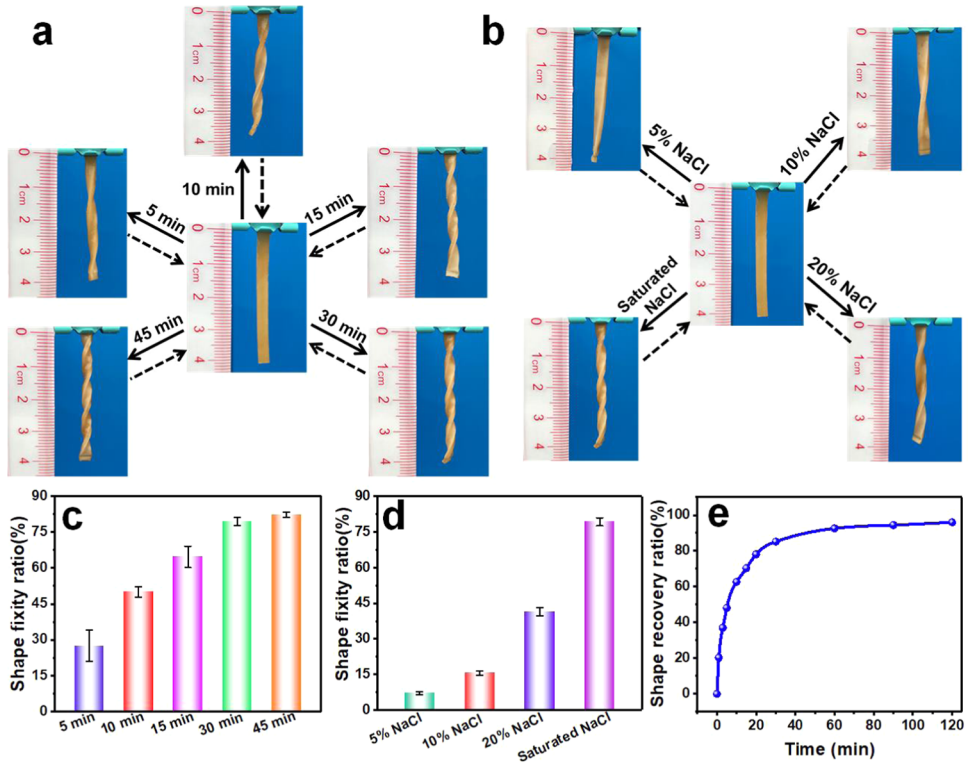

Figure 5. (a) Photographs of the temporary shapes of PVA−TA-30% hydrogels in saturated NaCl solution with time indication. (b) Photos of the temporary shapes of PVA−TA-30% hydrogels in different concentrations of NaCl solution (the curled angle was 900° and dashed lines indicate that the temporarily fixed shapes will be recovered in deionized water). Shape fixity ratios (R_f) of the hydrogels (c) with indicated times in saturated NaCl solution and (d) in different concentrations of NaCl solution. (e) Time-dependent shape recovery procedures in deionized water.

instance, with recent developments of stimuli polymers, shape-memory polymers have aroused increasingly more attention because of their promising applications in various field.[41] Inspired by the reversible physical interactions formed via soaking in NaCl solution, we use these newly formed physical interactions to stabilize temporary shapes. When immersed in water, these newly formed physical interactions could undergo disassociating process (Scheme 1a).

Shape fixity ratios of PVA−TA hydrogel increased with prolonging immersing time from about 27% for 5 min to maximum shape fixity ratios of about 80% for 30 and 45 min (Figure 5a,c). We fixed the fixity time at 30 min to investigate the effect of NaCl concentrations on the shape fixity ratios of PVA−TA hydrogels (Figure 5b,d). The concentrations of NaCl had an obvious effect on their shape fixity ratios. When the concentration was saturated, the fixed ratios of PVA−TA-30% hydrogel reach the maximum (about 80%). All of the fixed shapes could recover their original shapes when were transferred into deionized water (Figure 5e). In general, PVA−TA hydrogels have good shape-memory properties.

Properties and Applications of PVA-Based Hydrogels as Surgical Sutures. The flexible and biocompatible nature of the PVA−TA mixture is a suitable characteristic for surgical suture. In this study, a simple method was used to fabricate thread by injecting PVA−TA solution into NaCl solution (Scheme 1b). Interestingly, when injecting PVA−TA solution into other solvents such as water and ethanol, there was no thread formed (Figure S6 and Movie S3). These threads obtained from NaCl solution demonstrated good flexibility that could be coiled and knot-tightened (Figure 6a). Besides, they also showed a high failure strength and elongation of 13.4 MPa and 1000 ± 50%, respectively (Figure 6b). After stretching, the obtained PVA−TA-30% thread possessed ultrahigh tensile strength of 112 MPa accompanied with lower ductility (200 ± 20%) (Figure 6b), and it was so tough that could lift a weight of 1500 g (Figure 6b inset). Furthermore, the dried threads have ultrahigh failure tensile strength (737.4 and 16.6 MPa for stretched and unstretched dried threads, respectively) and good flexibility (Figure 6c and inset). By applying a stretching force, the stretched thread shows a record-high toughness and fracture strength among those reported tough materials (Scheme 1c).

For investigating whether the PVA/TA sutures meet the fundamental requirement in vivo, the I-10 cells were cultured on the dialyzed PVA/TA sutures, and the cell viability and proliferation were evaluated in vitro. As displayed in Figure 6d, the I-10 cells proliferated continuously on the PVA−TA-30% hydrogel (control group) and PVA/TA suture during the culture process. When the culture time reached 5 days, the I-10 cells showed almost entirely green fluorescence and good viability in visualizing live/dead staining florescent photographs (Figure 6e−g), confirming that the dialyzed PVA−TA sutures possessed good biocompatibility and cytocompatibility.

To demonstrate the applicability of the stretched PVA−TA thread as a surgical suture, we close an incision in an animal model using the following process: a mouse was sacrificed, shaved, and an incision was made. Subsequently, the stretched PVA−TA thread was used to suture the wound of the mouse with a standard surgical needle. During the entire procedure, the PVA−TA suture remained mechanically intact, and due to its flexible property, and the incision site was successfully closed with knotting (Figure 6h−j). The stability of PVA−TA

DOI: 10.1021/acs.biomac.9b01223
Biomacromolecules XXXX, XXX, XXX−XXX

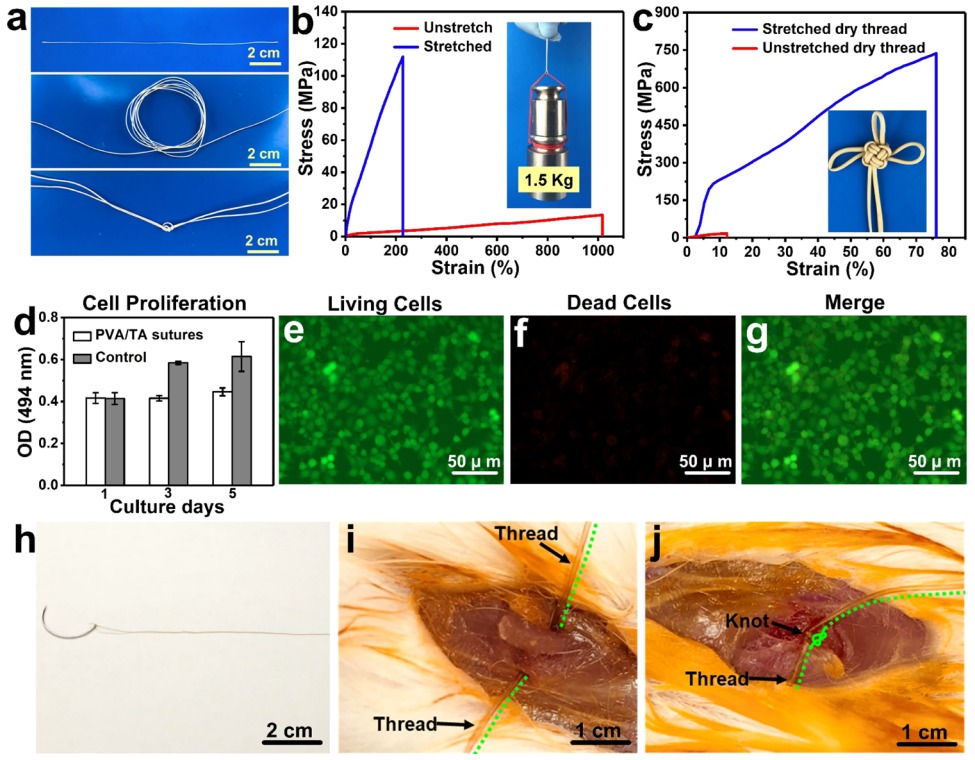

Figure 6. Photographs of (a) PVA–TA sutures with a diameter of 130 nm were coiled and knot-tightened. Tensile stress–strain curves of PVA–TA (b) wet sutures and (c) dry sutures with and without stretching. The inset in (b) shows that the thin stretched thread ($d \approx 0.51$ mm) was so tough that it could lift a weight of 1500 g. The inset in (c) shows that dry stretched PVA–TA sutures could be knitted to a "Chinese Knot". (d) Cell proliferation of the mouse Leydig tumor cells (I-10) on the surface of PVA–TA-30% hydrogel and PVA–TA sutures on days 1, 3, and 5. (e–g) Laser confocal images of cellular morphology on hydrogel after cultures for 5 days. (h–j) Photographs from the animal experiment showing that PVA–TA suture could be used for wound closure.

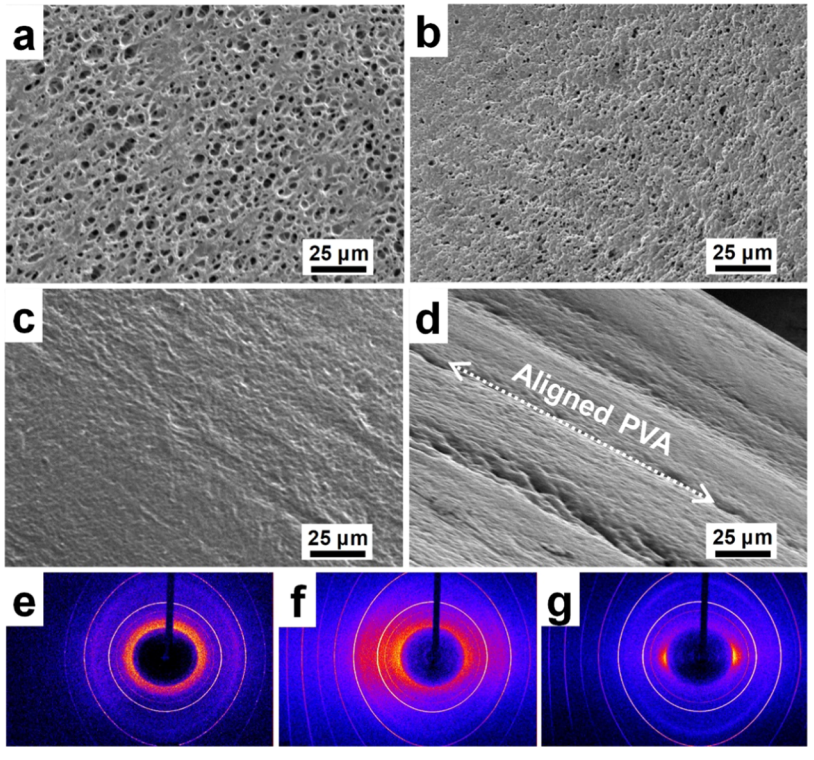

Figure 7. SEM images of cross sections of (a) unstretched and (b) stretched threads; axial surfaces of (c) unstretched and (d) stretched PVA–TA threads parallel to the stretching direction. Wide-angle X-ray 2D diffraction images of (e) unstretched saline-treated PVA–TA hydrogel, (f) unstretched PVA–TA, and (g) stretched PVA–TA threads.

DOI: 10.1021/acs.biomac.9b01223
Biomacromolecules XXXX, XXX, XXX–XXX

suture in vivo was also investigated by visualization through H&E staining. As demonstrated in Figure S7, the PVA−TA suture possessed effective tissue ligation capability after 6 days, indicating that the PVA−TA suture had suitable in vivo integrity for connecting incised tissues. Furthermore, at 3 days post implantation, the stained tissues showed infiltration of a few inflammatory cell around the PVA/TA suture (Figure S8). These results suggested that the PVA/TA sutures caused low immune responses in vivo. Thus, this facile, scalable, and time- and energy-efficient method for fabricating strong, stretchable, and biocompatible sutures has a great potential in the field of medicine.

Alignment Structures of PVA−TA Sutures. To identify the structure difference of stretched and unstretched PVA−TA sutures, the microstructures of the PVA−TA-30% threads before and after stretching are presented in Figure 7. The cross-sectional microstructure of the stretched thread shows a more denser porous structure (Figure 7b) than those unstretched thread (Figure 7a). We believe this reduced porosity structure of the stretched thread is mainly attributed to the thinner diameter after stretching along its axis direction. The axial surface microstructure of the unstretched thread shows a rough and uneven surface (Figure 7c), indicating no alignments produced. However, more "fiberlike" alignment structures appeared on the surface of the stretched thread (Figure 7d). The aligned structure of the stretched thread is expected to have strong contribution to the good mechanical properties.

Wide-angle X-ray 2D diffraction (WAXRD) shows that unstretched threads exhibit nearly randomly orientation patterns (Figure 7f), suggesting no orientation occurred. However, the stretched thread shows elliptical two-dimensional (2D) patterns, indicating the formation of well-aligned structures along the axis direction (Figure 7g). It is noteworthy that unstretched thread shows more ordered structure than unstretched hydrogels (Figure 7e,f), implying that the injecting process causes a slight alignment of PVA.

CONCLUSIONS

In summary, we used a facile route to prepare strong and tough PVA-based hydrogels through physical cross-linking and molecular alignment. In our work, saline-induced physical interactions act as "sacrificial domains" to effectively absorb energy and withstand large deformation. More remarkably, introducing reversible physical interactions to those hydrogels generated a new kind of stimuli shape-memory hydrogel, which was seldom achieved by the previously produced robust hydrogels. Due to its good cytotoxicity and biocompatibility, we explored the application of the PVA-based threads as surgical sutures to close an incision of a mouse. In addition, by a straightforward injecting and stretching method, we fabricated PVA−TA thread with aligned structures. Compared to its counterpart, the aligned PVA−TA thread leads to a dramatic increase in mechanical strength and toughness. The alignment of the threads was further confirmed by SEM and WXRD analysis. This study not only develops a strong, stretchable, and biocompatible hydrogel but also created new applications as memorizing temporary shapes and closing an incision as a surgical suture. We anticipate that this work will open doors to producing PVA−TA-based multifunctional products for biorelated applications.

ASSOCIATED CONTENT

Supporting Information

The Supporting Information is available free of charge on the ACS Publications website at DOI: 10.1021/acs.biomac.9b01223.

M1 hydrogel bounced and hit like a ping-pong ball (MOV)

M2 Hydrogel tube were repeated browned (MOV)

M3 Wet-drawing PVA−TA mixtures in different solvents (MOV)

Images of PVA−TA-30% and PVA−TA-0% hydrogels before and after immersing in saturated NaCl solution; compressive stress−strain curves and swelling ratios of the PVA−TA-0% and PVA−TA-30% before and after immersed in NaCl solution; images of the PVA−TA-30% and PVA−TA-30%-S-NaCl and PVA−TA-0% and PVA−TA-0%-S-NaCl hydrogels in the swelling process; tensile stress−strain curves of PVA hydrogels with different TA concentrations before and after immersed in saturated NaCl solution for 12 h; elastic modulus and toughness of PVA−TA hydrogels before and after immersed in saturated NaCl solution; tensile stress−strain curves, elastic moduli, and toughnesses of PVA−TA-30%-S-NaCl hydrgoels with different cycles of freezing/thawing treatment; tensile stress−strain curves, elastic moduli, and toughnesses of PVA−TA-30%-y-NaCl hydrogels with different immersing times, and immersed in different concentrations of NaCl solutions; wet-drawing PVA−TA mixtures in NaCl solution, water, and ethanol; H&E stained images of wounding closing sites with PVA−TA sutures after 6 days; and connective tissue around the implanted PVA/TA sutures (PDF)

AUTHOR INFORMATION

Corresponding Author

*E-mail: h.zhu@neu.edu.

Author Contributions

⊥W.C. and N.L. contributed equally to this work.

Notes

The authors declare no competing financial interest.

ACKNOWLEDGMENTS

This work was supported by Northeastern University startup, international cooperation program for key professors, Qufu Normal University, and international program for Ph.D. candidates, South University of Technology, National Natural Science Foundation of China (No. 21808126). The authors thank Prof. Livemore Carol in Northeastern University for providing mechanical test machine (Instron Model 5567), Prof. Jinhui Xu in Qufu Normal University for in vivo experiment, and Dr. Meiling Yu from the First Affiliated Hospital of Bengbu Medical College for the cell cultivation experiment.

REFERENCES

(1) Lee, K. Y.; Mooney, D. J. Hydrogels for Tissue Engineering. *Chem. Rev.* **2001**, *101*, 1869−1879.

(2) Drury, J. L.; Mooney, D. J. Hydrogels for Tissue Engineering:Scaffold Design Variables and Applications. *Biomaterials* **2003**, *24*, 4337−4351.

(3) Hoare, T. R.; Kohane, D. S. Hydrogels in Drug Delivery: Progress and Challenges. *Polymer* **2008**, *49*, 1993−2007.

DOI: 10.1021/acs.biomac.9b01223
Biomacromolecules XXXX, XXX, XXX−XXX

(4) Qiu, Y.; Park, K. Environment-Sensitive Hydrogels for Drug Delivery. *Adv. Drug Delivery Rev.* **2001**, *53*, 321−339.
(5) Larson, C.; Peele, B.; Li, S.; Robinson, S.; Totaro, M.; Beccai, L.; Mazzolai, B.; Shepherd, R. Highly Stretchable Electroluminescent Skin for Optical Signaling and Tactile Sensing. *Science* **2016**, *351*, 1071−1074.
(6) Ionov, L. Hydrogel-Based Actuators: Possibilities and Limitations. *Mater. Today* **2014**, *17*, 494−503.
(7) Gong, J. P. Materials Both Tough and Soft. *Science* **2014**, *344*, 161−162.
(8) Sakai, T.; Akagi, Y.; Matsunaga, T.; Kurakazu, M.; Chung, U. I.; Shibayama, M. Highly Elastic and Deformable Hydrogel Formed From Tetra-Arm Polymers. *Macromol. Rapid Commun.* **2010**, *31*, 1954−1959.
(9) Yang, Y.; Wang, X.; Yang, F.; Wang, L.; Wu, D. Highly Elastic and Ultratough Hybrid Ionic-Covalent Hydrogels with Tunable Structures and Mechanics. *Adv. Mater.* **2018**, No. 1707071.
(10) Zhao, D.; Huang, J.; Zhong, Y.; Li, K.; Zhang, L.; Cai, J. High Strength and High Toughness Double Cross Linked Cellulose Hydrogels: A New Strategy Using Sequential Chemical and Physical Cross-Linking. *Adv. Funct. Mater.* **2016**, *26*, 6279−6287.
(11) Haraguchi, K.; Takehisa, T. Nanocomposite Hydrogels: A Unique Organic−Inorganic Network Structure with Extraordinary Mechanical, Optical, and Swelling/De-Swelling Properties. *Adv. Mater.* **2002**, *14*, 1120−1124.
(12) Mayumi, K.; Tezuka, M.; Bando, A.; Ito, K. Mechanics of Slide-Ring Gels: Novel Entropic Elasticity of a Topological Network Formed by Ring and String. *Soft Matter* **2012**, *8*, 8179−8183.
(13) Morrow, D. A.; Donahue, T. L. H.; Odegard, G. M.; Kaufman, K. R. Transversely Isotropic Tensile Material Properties of Skeletal Muscle Tissue. *J. Mech. Behav. Biomed. Mater.* **2010**, *3*, 124−129.
(14) Danso, E. K.; Honkanen, J. T. J.; Saarakkala, S.; Korhonen, R. K. Comparison of Nonlinear Mechanical Properties of Bovine Articular Cartilage and Meniscus. *J. Biomech.* **2014**, *47*, 200−206.
(15) Mredha, M. T. I.; Guo, Y. Z.; Nonoyama, T.; Nakajima, T.; Kurokawa, T.; Gong, J. P. A Facile Method to Fabricate Anisotropic Hydrogels with Perfectly Aligned Hierarchical Fibrous Structures. *Adv. Mater.* **2018**, *30*, No. 1704937.
(16) Wu, Y.; Shah, D. U.; Liu, C.; Yu, Z.; Liu, J.; Ren, X.; Rowland, M. J.; Abell, C.; Ramage, M. H.; Scherman, O. A. Bioinspired Supramolecular Fibers Drawn From a Multiphase Self-Assembled Hydrogel. *Proc. Natl. Acad. Sci. U.S.A.* **2017**, *114*, 8163.
(17) Liu, T.; et al. Super-Strong and Tough Poly(Vinyl Alcohol)/Poly(Acrylic Acid) Hydrogels Reinforced by Hydrogen Bonding. *J. Mater. Chem. B* **2018**, *6*, 8105−8114.
(18) Guo, G.; Chen, Y.; Liu, X.; Zhu, D. Y.; Gao, L. Tough and Durable Hydrogels with Robust Skin Layers Formed Via a Soaking Treatment *J. Mater. Chem. B* 2018, *648* DOI: 10.1039/C8TB02540A.
(19) Li, X.; Zhao, Y.; Li, D.; Zhang, G.; Long, S.; Hui, W. Hybrid Dual Crosslinked Polyacrylic Acid Hydrogels with Ultrahigh Mechanical Strength, Toughness and Self-Healing Properties Via Soaking Salt Solution. *Polymer* **2017**, *121*, 55−63.
(20) Baker, M. I.; Walsh, S. P.; Schwartz, Z.; Boyan, B. D. A Review of Polyvinyl Alcohol and its Uses in Cartilage and Orthopedic Applications. *J. Biomed. Mater. Res., Part B* **2012**, *100B*, 1451−1457.
(21) Lopes, G. K.; Schulman, H. M.; Hermes-Lima, M. Polyphenol Tannic Acid Inhibits Hydroxyl Radical Formation From Fenton Reaction by Complexing Ferrous Ions. *Biochim. Biophys. Acta* **1999**, *1472*, 142−152.
(22) Fan, H.; Wang, J.; Jin, Z. Tough, Swelling-Resistant, Self-Healing, and Adhesive Dual-Cross-Linked Hydrogels Based On Polymer−Tannic Acid Multiple Hydrogen Bonds. *Macromolecules* **2018**, *51*, 1696−1705.
(23) Fan, H.; Wang, L.; Feng, X.; Bu, Y.; Wu, D.; Jin, Z. Supramolecular Hydrogel Formation Based On Tannic Acid. *Macromolecules* **2017**, *50*, 666−676.
(24) Zhu, Z.; Ling, S.; Yeo, J.; Zhao, S.; Tozzi, L.; Buehler, M. J.; Omenetto, F.; Li, C.; Kaplan, D. L. High-Strength, Durable All-Silk Fibroin Hydrogels with Versatile Processability Toward Multifunctional Applications. *Adv. Funct. Mater.* **2018**, *28*, No. 1704757.
(25) Xu, D.; Huang, J.; Zhao, D.; Ding, B.; Zhang, L.; Cai, J. High Flexibility, High Toughness Double Cross Linked Chitin Hydrogels by Sequential Chemical and Physical Cross-Linkings. *Adv. Mater.* **2016**, *28*, 5844−5849.
(26) He, Q.; Huang, Y.; Wang, S. Hofmeister Effect Assisted One Step Fabrication of Ductile and Strong Gelatin Hydrogels. *Adv. Funct. Mater.* **2018**, *28*, No. 1705069.
(27) Yang, Y.; Wang, X.; Yang, F.; Shen, H.; Wu, D. A Universal Soaking Strategy to Convert Composite Hydrogels Into Extremely Tough and Rapidly Recoverable Double-Network Hydrogels. *Adv. Mater.* **2016**, *28*, 7178−7184.
(28) Chen, Y. N.; Peng, L.; Liu, T.; Wang, Y.; Shi, S.; Wang, H. Poly(Vinyl Alcohol)-Tannic Acid Hydrogels with Excellent Mechanical Properties and Shape Memory Behaviors. *ACS Appl. Mater. Interfaces* **2016**, *8*, 27199.
(29) Li, G.; Zhang, H.; Fortin, D.; Xia, H.; Zhao, Y. Poly (Vinyl Alcohol)-Poly (Ethylene Glycol) Double-Network Hydrogel: A General Approach to Shape Memory and Self-Healing Functionalities. *Langmuir* **2015**, *31*, 11709−11716.
(30) Kong, W.; Wang, C.; Jia, C.; Kuang, Y.; Pastel, G.; Chen, C.; Chen, G.; He, S.; Huang, H.; Zhang, J.; Wang, S.; Hu, L. Muscle-Inspired Highly Anisotropic, Strong, Ion-Conductive Hydrogels. *Adv. Mater.* **2018**, *0*, No. 1801934.
(31) You, J.; Xie, S.; Cao, J.; Ge, H.; Xu, M.; Zhang, L.; Zhou, J. Quaternized Chitosan/Poly(Acrylic Acid) Polyelectrolyte Complex Hydrogels with Tough, Self-Recovery, and Tunable Mechanical Properties. *Macromolecules* **2016**, *49*, 1049−1059.
(32) Luo, F.; Sun, T. L.; Nakajima, T.; Kurokawa, T.; Zhao, Y.; Sato, K.; Ihsan, A. B.; Li, X.; Guo, H.; Gong, J. P. Oppositely Charged Polyelectrolytes Form Tough, Self-Healing, and Rebuildable Hydrogels. *Adv. Mater.* **2015**, *27*, 2722−2727.
(33) Wang, J.; Satoh, M. Novel PVA-Based Polymers Showing an Anti-Hofmeister Series Property. *Polymer* **2009**, *50*, 3680−3685.
(34) Nostro, P. L.; Ninham, B. W. Hofmeister Phenomena: An Update on Ion Specificity in Biology. *Chem. Rev.* **2012**, *112*, 2286−2322.
(35) Zhao, X. Multi-Scale Multi-Mechanism Design of Tough Hydrogels: Building Dissipation Into Stretchy Networks. *Soft Matter* **2014**, *10*, 672−687.
(36) Dai, L.; Kohshuke, U.; Mohammad, S. S.; Kazuo, Y. Gelation of a new hydrogel system of Atactic-Poly (vinyl alcohol)/NaCl/H_2O. *Polym. Int.* **2002**, *51*, 715−720.
(37) Peng, S.; Liu, S.; Sun, Y.; Xiang, N.; Jiang, X.; Hou, L. Facile preparation and characterization of poly (vinyl alcohol)-NaCl-glycerol supramolecular hydrogel electrolyte. *Eur. Polym. J.* **2018**, *106*, 206−213.
(38) Bian, H.; Wei, L.; Lin, C.; Ma, Q.; Dai, H.; Zhu, J. Y. Lignin Containing Cellulose Nanofibril-Reinforced Polyvinyl Alcohol Hydrogels. *ACS Sustainable Chem. Eng.* **2018**, *6*, 4821−4828.
(39) He, Z.; Alexandridis, P. Micellization Thermodynamics of Pluronic P123 (EO20PO70EO20) Amphiphilic Block Copolymer in Aqueous Ethylammonium Nitrate (EAN) Solutions. *Polymers* **2017**, *10*, No. 32.
(40) Gong, Z.; Zhang, G.; Zeng, X.; Li, J.; Li, G.; Huang, W.; Sun, R.; Wong, C. High-Strength, Tough, Fatigue Resistant, and Self-Healing Hydrogel Based On Dual Physically Cross-Linked Network. *ACS Appl. Mater. Interfaces* **2016**, *8*, 24030−24037.
(41) Lu, W.; Le, X.; Zhang, J.; Huang, Y.; Chen, T. Supramolecular Shape Memory Hydrogels:A New Bridge between Stimuli-Responsive Polymers and Supramolecular Chemistry. *Chem. Soc. Rev.* **2017**, *46*, 1284.

DOI: 10.1021/acs.biomac.9b01223
Biomacromolecules XXXX, XXX, XXX−XXX